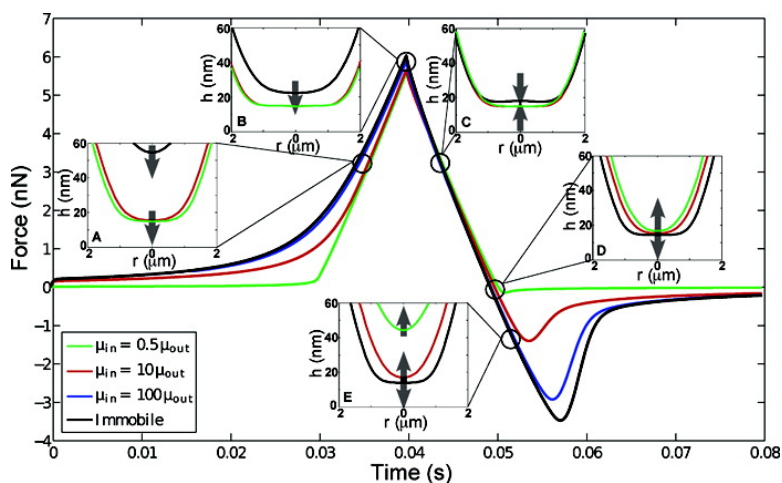**Letter**

Effects of Internal Flow and Viscosity Ratio on Measurements of Dynamic Forces between Deformable Drops

Scott A. Edwards, Steven L. Carnie, Ofer Manor, and Derek Y. C. Chan

More About This Article

Additional resources and features associated with this article are available within the HTML version:

- Supporting Information
- Access to high resolution figures
- Links to articles and content related to this article
- Copyright permission to reproduce figures and/or text from this article

View the Full Text HTML

Effects of Internal Flow and Viscosity Ratio on Measurements of Dynamic Forces between Deformable Drops

Scott A. Edwards,[†] Steven L. Carnie,[†] Ofer Manor,[†] and Derek Y. C. Chan*,[†,‡]

*Particulate Fluids Processing Centre and Department of Mathematics and Statistics,
The University of Melbourne, Parkville, Victoria, 3010, Australia, and Department of Mathematics,
National University of Singapore, 117543, Singapore*

A model that has been shown to give very accurate predictions of dynamic forces between deformable emulsion drops and bubbles is used to quantify the effects of internal flow and viscosity ratio on the hydrodynamic interaction in such systems. The results demonstrate that direct force measurement using an atomic force microscope can readily differentiate whether the interfaces of drops of different viscosities respond as immobile (no-slip) or fully mobile (no tangential shear stress) boundaries.

When emulsion drops approach each other at low speeds, they interact via the disjoining pressure Π due to, for example, electrical double layer and van der Waals interactions. At separations where the magnitude of the disjoining pressure becomes comparable to the Laplace pressures ΔP of the drops, the drops will deform: either flattening if Π is repulsive or pimpling and eventually coalescing if Π is attractive.[1] At higher velocities, hydrodynamic pressure p in the thin film between the drops also becomes important and gives rise to a repulsive dynamic force if the drops are pushed together, or an attractive force if they are pulled apart. At sufficiently high velocities, the hydrodynamic pressure can exceed the Laplace pressure when the drops approach, and the film will form the characteristic hydrodynamic dimple.[2,3] The magnitude of p depends crucially on the hydrodynamic boundary condition at the drop–solvent interface as well as on any deformations of the interface.

Results of recent atomic force microscope (AFM) measurements of dynamic forces between two micrometer-sized oil droplets interacting in water in their typical Brownian velocity range were consistent with a model that treated the drop surfaces as immobile so that a no-slip hydrodynamic boundary condition applies at the drop interface.[4] This was appropriate in the context of these experiments, as surfactant had been added to stabilize the oil drops at a high enough concentration to effectively immobilize the oil–water interface. The no-slip, hydrodynamically immobile interface also means that there is no need to solve for flow inside the drops. However, there may be situations, such as in nonaqueous systems[5] in which the drop–solvent interface is clean and mobile; then, instead of a zero-velocity boundary condition, there is continuity of stress across the interface. Correct treatment of such a system requires solving for the flow induced within the drop by stresses generated at the drop surface.

At the level of the lubrication approximation, the boundary integral form of the Stokes equation for flow inside the drop can be solved using the Greens function kernel derived by Jansons and Lister.[6] This formulation gives a direct relation between the surface stress and the tangential fluid velocity at the drop surface. Davis et al.[7] applied this method to the case of nondeformable interacting drops, and studied how the asymptotic force-separation scaling changes with the ratio of drop viscosity to solvent viscosity. This formulation has since been applied to the case of deformable drops interacting at constant force,[2,8,9] at constant velocity,[9,10] under a time-varying interaction force,[11] and in the presence of external flow fields.[12,13]

The AFM experiments we wish to model here are not described by this previous work, in that the dynamic interaction forces are directly measured, the device compliance or spring constant is part of the model, and drops are typically brought into contact, then pulled apart with a set velocity schedule. In this paper, we study the influence of the mobility of the drop interface on drop deformation and measured force under typical AFM experimental conditions.

The model calculates the thickness $h(r,t)$ of the axisymmetric thin film separating two identical drops of unperturbed radius R_0, surface tension σ, surface potential ψ, contact angle θ_c and viscosity μ_{in}, immersed in a solvent of viscosity μ_{out}. In the typical AFM experimental configuration, one drop is adsorbed on a solid substrate, and the other is attached to a cantilever with spring constant K (see the inset to Figure 2). The governing equations are[2,9]

$$\frac{\sigma}{2r}\frac{\partial}{\partial r}\left(r\frac{\partial h}{\partial r}\right) = \frac{2\sigma}{R_0} - (p + \Pi) \tag{1}$$

$$\frac{\partial h}{\partial t} = \frac{1}{12\mu_{out}r}\frac{\partial}{\partial r}\left(rh^3\frac{\partial p}{\partial r}\right) - \frac{1}{r}\frac{\partial}{\partial r}(rUh) \tag{2}$$

Equation 1 is the augmented Young–Laplace equation relating the film thickness to spatial variations in the hydrodynamic

* Corresponding author. E-mail: D.Chan@unimelb.edu.au.
† The University of Melbourne.
‡ National University of Singapore.
(1) Miklavcic, S. J.; Attard, P. *J. Phys. A: Math. Gen.* **2002**, *35*, 4335.
(2) Yiantsios, S. G.; Davis, R. H. *J. Fluid Mech.* **1990**, *217*, 547.
(3) Błwazdziewicz, J.; Wajnryb, E.; Loewenberg, M. *J. Fluid Mech.* **1999**, *395*, 29.
(4) Dagastine, R. R.; Manica, R.; Carnie, S. L.; Chan, D. Y. C.; Stevens, G. W.; Grieser, F. *Science* **2006**, *313*, 210.
(5) Yoon, Y.; Borrell, M.; Park, C. C.; Leal, L. G. *Phys. Fluids* **2005**, *16*, 3945.
(6) Jansons, K. M.; Lister, J. R. *Phys. Fluids* **1988**, *31*, 1321.
(7) Davis, R. H.; Schonberg, J. A.; Rallison, J. M. *Phys. Fluids* **1989**, *1*, 77.
(8) Saboni, A.; Gourdon, C.; Chesters, A. K. *J. Colloid Interface Sci.* **1995**, *175*, 27.
(9) Bazhlekov, I. B.; Chesters, A. K.; van de Vosse, F. N. *Int. J. Multiphase Flow* **2006**, *26*, 445.
(10) Abid, S.; Chesters, A. K. *Int. J. Multiphase Flow* **1994**, *20*, 613.
(11) Rother, M. A.; Zinchenko, A. Z.; Davis, R. H. *J. Fluid Mech.* **1997**, *346*, 117.
(12) Nemer, M. B.; Chan, X.; Papadopoulos, D. H.; Błwazdziewicz, J.; Loewenberg, M. *Phys. Rev. Lett.* **2004**, *92*, 114501.
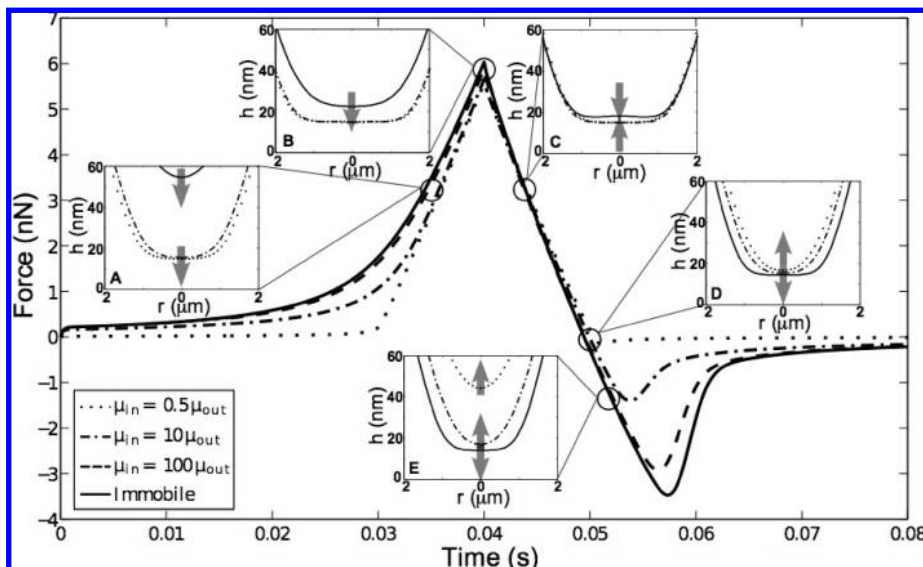(13) Baldessari, F.; Leal, L. G. *Phys. Fluids* **2006**, *18*, 013602.

Figure 1. Calculated force curves for two drops driven together at a speed of $V = 50$ μm/s for a time of 40 ms, then pulled apart at the same speed, for viscosity ratios $\mu_{in}/\mu_{out} = 0.5$ ($\cdots$), 10 ($-\cdot-$), 100 ($---$) and ∞ (i.e., immobile interface) ($-$). Other drop properties are given in the main text. Note that the drops would collide at $t = 30$ ms if they were not deformable. The insets show drop separation profiles $h(r,t)$ for the three cases $\mu_{in}/\mu_{out} = 0.5$, 10, and ∞ (immobile interface) at different times: (A) $t = 34$ ms, (B) $t = 40$ ms, (C) $t = 45$ ms, (D) $t = 50$ ms, and (E) $t = 51$ ms. The vertical arrows indicate whether the central drop separation is increasing (up) or decreasing (down).

pressure p and disjoining pressure Π within the thin film. Deformation is assumed to be small compared to R_0, and gradients of the drop shape in the radial direction are assumed to be small compared to unity. The interfacial tension is taken to be constant in eq 1. This assumption is reasonable, as we are concerned only with the effects of different hydrodynamic boundary conditions. However, if, for example, the Marangoni effect is the subject of interest, then gradients in interfacial tension would need to be considered. Equation 2 describes the thinning or thickening of the film as the drops approach or retract, and follows from Reynolds lubrication theory. The first term corresponds to the parabolic component of the flow field driven by pressure gradients, while the second term relates to plug flow arising from the tangential flow velocity U generated at the drop surfaces.[7] The second term is not present if the drop surfaces are immobile.

The interfacial velocity U can be calculated using the boundary integral formulation of the Stokes equation[6,7]

$$U(r) = -\frac{1}{2\mu_{in}} \int_0^\infty \phi(r,\rho) h(\rho) \frac{\partial p}{\partial \rho} d\rho \qquad (3)$$

where the Greens function kernel φ at the level of the lubrication approximation (i.e., neglecting the curvature of the drop surfaces) is given by[6]

$$\phi(r,\rho) = \frac{\rho}{2\pi} \int_0^\pi \frac{\cos\theta}{\sqrt{r^2 + \rho^2 - 2r\rho\cos\theta}} d\theta \qquad (4)$$

Equations 1$-$4 are solved numerically out to a distance $r_{max} \sim R_0/3$ from the center, with a boundary condition given by an analytic solution for the outer part of the drop that incorporates the driven motion of the drop, the displacement of the AFM

piezoelectric motor $\Delta X(t)$, and the deflection of the cantilever $\Delta s(t) = F/K$[14,15]

$$\frac{dX}{dt} = \frac{\partial h}{\partial t} + \frac{\alpha}{2\pi\sigma}\frac{dF}{dt} \qquad \text{at} \quad r = r_{max} \qquad (5a)$$

$$\alpha = \ln\left(\frac{r_{max}^2}{4R_0^2}\right) + 2 + \ln\left(\frac{1+\cos\theta_c}{1-\cos\theta_c}\right) - \frac{2\pi\sigma}{K} \qquad (5b)$$

where $F(t) = 2\pi \int_0^\infty r[p(r,t) + \Pi(r,t)]dr$ is the total force between the drops and θ_c is the contact angle of the drops. The use of the boundary condition in eqs 5 is the key difference between our model for AFM experiments and previous work.

We illustrate the physical implications of this model by choosing parameters typical of an AFM drop$-$drop experiment for an oil-in-water emulsion, but taken to be clean and surfactant-free. Two drops are placed initially at a separation of $h(r = 0, t = 0) = 1.5$ μm. The AFM motor then drives the drops together at a constant velocity $V = -dX/dt = 50$ μm/s, for a total displacement $\Delta X = 2$ μm. Then the motor is reversed, and the drops are retracted to their original separation at the same speed. Note that the drops are pushed 0.5 μm beyond the point at which they would come into contact if they were unable to deform. The drops have radii of $R_0 = 40$ μm, surface tension of $\sigma = 20$ mN/m, and surface electrostatic potential $\Psi = -30$ mV, the bulk fluid has an electrolyte concentration of $c_0 = 10$ mM, and the contact angle θ_c in eq 5b is taken to be 90° for simplicity (see Figure 2). With these parameters, the repulsive double layer disjoining pressure Π (calculated in the superposition approximation) balances the Laplace pressure $2\sigma/R_0$ of the drops at a separation $h \approx 15$ nm, at which distance the van der Waals interaction is negligible. This separation corresponds to about 5 Debye lengths so that the use of the superposition approximation is self-consistent. This also means that, during such interactions, deformations of the drops are more important than any effect on

(14) Manica, R.; Connor, J. N.; Dagastine, R. R.; Carnie, S. L.; Horn, R. G.; Chan, D. Y. C. *Phys. Fluids* **2008**, *20*, 032101.

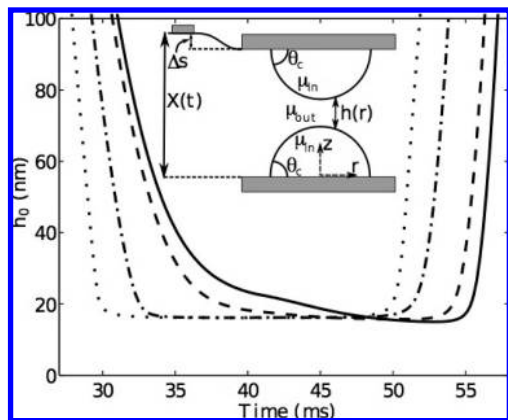(15) Carnie, S. L.; Chan, D. Y. C.; Lewis, C.; Manica, R.; Dagastine, R. R. *Langmuir* **2005**, *21*, 2912.

Figure 2. The central drop-drop separation $h_0(t) \equiv h(r = 0, t)$ calculated for the same approach−retract runs addressed in Figure 1. The four cases are $\mu_{in}/\mu_{out} = 0.5$ (···), 10 (−·−), 100 (− − −), and ∞ (i.e., immobile interface) (−). At time $t = 40$ ms, the direction of the AFM drive is reversed from approach to retract. The inset schematic defines the geometry of the system.

the state of the electrical double layer beyond that of a drop in isolation. The viscosity of the bulk fluid μ_{out} is set to that of water, while a range of values for the drop viscosity μ_{in} are considered to illustrate the influence of viscosity ratio and drop deformations on hydrodynamic interactions.

Force curves corresponding to four cases are shown in Figure 1. The conditions for each case were identical except for the value of the drop viscosity μ_{in}. The solid curve corresponds to the drop surfaces being immobile, and the no-slip boundary condition holds, which is equivalent to $\mu_{in} \rightarrow \infty$. The asymmetry of the force curves, which is solely a consequence of hydrodynamics, diminishes markedly as μ_{in} is reduced; this is most apparent around $t = 55$ ms, in the vicinity of the attractive force minimum arising from hydrodynamic suction as the drops are pulled apart. For the smallest value of the drop viscosity, $\mu_{in} = 0.5\mu_{out}$, there is only the barest hint of any hydrodynamic influence on the force curve, and in fact the curve is indistinguishable from an equilibrium force curve measured at a far slower drive speed.

Drop separation profiles $h(r,t)$ are shown for five different moments during the run, for the $\mu_{in} = 0.5\mu_{out}$, $\mu_{in} = 10\mu_{out}$, and immobile interface (no-slip) cases. From examining the profiles at times A (35 ms) and B (40 ms), on the approach branch of the force curve, it is clear that the separation between the no-slip drops decreases much more slowly than for the low-viscosity drops. At time A, when the total force is at half its maximum, the no-slip drops are still separated by over 55 nm, while the low-viscosity drops are already flattening against the disjoining pressure at $h \approx 15$ nm. At time C (45 ms), just after the reversal of the drive, a dimple has formed between the no-slip drops. The drainage of the dimple is still not complete by time D (50 ms), around which time the net force between the drops is zero because repulsion due to electrical double layer interactions is balanced by attraction from hydrodynamic interactions between the retracting interfaces. At time E (51 ms) the film between the no-slip drops is still thinning, but meanwhile the low-viscosity drops are steadily separating.

The time course of the thin-film drainage is illustrated another way in Figure 2, in which the central drop−drop separation at $h_0 \equiv h(r = 0, t)$ is plotted as a function of time. At one extreme is the curve for the $\mu_{in} = 0.5\mu_{out}$ case. The drops remain undeformed until $t = 30$ ms, the time at which they would collide if they could not deform. Thereafter, they simply flatten against the repulsive disjoining pressure until 10 ms after drive reversal

when they start to separate again, following a trajectory that is the mirror image of the approach. At the other extreme, the curve for the no-slip drops is highly asymmetrical around $t = 40$ ms, as the centers of the drops are dimpled during the approach. The dimple continues to drain for 10 ms after the drive is reversed, and only after an additional 5 ms do the drops finally separate. The curves for other finite values of μ_{in} fall between these two extremes.

The marked differences between force curves and film profiles predicted for low-viscosity and no-slip drops ultimately rest on the relative importance of the hydrodynamic pressure in the thin film. For no-slip or high-viscosity drops, the resistance to fluid flowing in or out of the film is high, so hydrodynamic pressure plays an important role. For low-viscosity drops, the drop surfaces provide very little resistance to film flow, and the hydrodynamic pressure in the film is negligible. Davis et al.[6] showed using a scaling argument that these two regimes can be classified according to the mobility number $m \equiv (\mu_{out}/\mu_{in})(R_0/h_0)^{1/2}$. For $m \gg 1$, the drop surface is effectively fully mobile, and behaves like a free surface that cannot sustain any stress; for $m \ll 1$, it is effectively immobile, and behaves like a no-slip boundary. For our system, with drop radius $R_0 = 40$ μm and minimum separation $h_0 \approx 15$ nm, the crossover between the two regimes at $m = 1$ corresponds to a drop viscosity $\mu_{in} = 50\mu_{out}$. This is consistent with our findings that one must have $\mu_{in} > 100\mu_{out}$ for the behavior to approach that of the no-slip case. For $\mu_{in} \sim \mu_{out}$, which is often the case in typical experiments, $m \sim 10^2$, and thus the drop surfaces are effectively fully mobile; accordingly, our calculations show negligible hydrodynamic effects in this regime. Since m depends only weakly on drop radius R_0, our conclusion is that, for fully mobile and deformable interfaces, hydrodynamic forces are negligible when $\mu_{in} \sim \mu_{out}$, over the range of drop sizes accessible to AFM manipulation. This is consistent with the prediction of Davis et al.[7] for interaction involving interaction between rigid surfaces, and with previous studies under constant force or constant velocity conditions.[9]

From the point of view of simply fitting experimental force curves that may correspond to the fully mobile interface, it is possible to circumvent having to consider effects of fluid flow inside the drops by using the Navier slip model which assumes the boundary condition $U = b(dU/dr)$ holds at the interface with the slip length b as a fitting parameter. In the present calculation, we found that $b = 100$ nm will roughly mimic the force curves and drop profiles for the case $\mu_{in} = 10\mu_{out}$ or $b = 2.3$ μm for $\mu_{in} = 0.5\mu_{out}$. However, while being able to fit force data, there is no direct connection between the fitted slip length and the fluid properties of the drops.

We have presented simulation results under typical AFM conditions for the dynamic force and interfacial deformations that arise during interaction between deformable viscous drops that have fully mobile interfaces. The model takes into account the continuity of tangential stress across the drop interface and fluid flow inside the drop and predicts large variations in the measured force curves and the drop separation profiles with the viscosity ratio. The magnitude of hydrodynamic forces characteristic of immobile drop interfaces are manifest only when the drop viscosities exceed about 100 times the solvent viscosity. Conversely, for drop viscosities of the same order as the solvent viscosity, hydrodynamic forces are found to be negligible, and the resulting force curves are almost indistinguishable from equilibrium response, even at the highest accessible drive speeds. Any observed hydrodynamic force for such low-viscosity drops must be due to other factors, such as contaminant that immobilizes the interface.

Thus the measurement of dynamic forces between drops constitutes a very sensitive probe of the conditions at the drop−solvent interface. Indeed, recent force measurements involving clean bubbles in electrolyte solutions suggest that trace amounts of contaminants are sufficient to render the air/water interface to behave more like a no-slip surface than a fully mobile interface.[16] This is further supported by recent bubble rise studies in aqueous electrolytes where the Hadamard−Rybczynski result for the terminal velocity of bubbles with the fully mobile boundary condition is only observed if the electrolyte is cleaned very rigorously by sparging with clean N_2 for at least 1 h.[17] Even

under carefully controlled conditions, such results will only persist for about 30 min because contaminants will cause the boundary condition to change from fully mobile to partially mobile or immobile.

(16) Manor, O.; Vakarelski, I. U.; Tang, X.; O'Shea, S. J.; Stevens, G. W.; Grieser, F.; Dagastine, R. R.; Chan, D. Y. C. *Phys. Rev. Lett.* **2008**, *101*, 024501.
(17) Henry, C. L.; Luke Parkinson, L.; Ralston, J. R.; Craig, V. J. S. *J. Phys. Chem. C* **2008**, *112*, 15094.